

Quark model approach to the η meson electroproduction on the proton

Qiang Zhao^{1,2*}, Bijan Saghai³, and Zhenping Li⁴

1) *Department of Physics, University of Surrey, Guildford, Surrey GU2 7XH, United Kingdom*

2) *Institut de Physique Nucléaire, F-91406 Orsay Cedex, France*

3) *Service de Physique Nucléaire, DSM/DAPNIA, CEA/Saclay,
F-91191 Gif-sur-Yvette, France*

4) *Department of Physics, Peking University, 100871 Beijing, P.R. China*

Abstract

A recently developed quark model approach to pseudoscalar meson photo-production is extended to electroproduction process for the η meson in the kinematics of momentum transfer $Q^2 \leq 4$ (GeV/c)² and total center of mass energy $W \leq 1.6$ GeV. Existing data are well reproduced and the roles of the $S_{11}(1535)$ and $D_{13}(1520)$ resonances are closely investigated. In the study of the longitudinal excitation of the $S_{11}(1535)$ resonance, a reliable constraint on the $S_{11}(1535)$ properties is obtained by cleanly removing the electromagnetic transition from the $\gamma_{(v)}p \rightarrow S_{11}(1535) \rightarrow \eta p$ amplitude. Thus, the fitted quantities can be determined with an uncertainty of about 15%. This could be the first direct constraint on the $S_{11}(1535)$ properties in theory.

PACS number(s): 12.39.-x, 13.60.-r, 13.60.Le, 14.20.Gk

*Electronic address: qiang.zhao@surrey.ac.uk

I. INTRODUCTION

Our knowledge about the internal structures of baryon resonances, which generally belong to non-perturbative QCD phenomena, are still far from complete. Nowadays, with the availabilities of high intensity photon and electron beams at JLab, ESRF, MAMI, ELSA, and SPring-8, the baryon resonances thus can be systematically investigated via meson photo- and electroproduction. This initiates various theoretical efforts, through which one expects that our knowledge about these non-perturbative phenomena can be established on a more solid and fundamental ground.

In the late 1990's, experimental data with unprecedented accuracies were available for the η meson photoproduction which allowed a close study of resonance excitations in $\gamma_{(v)}p \rightarrow \eta p$. For example, the photoproduction data for the cross sections and single polarization observables obtained at MAMI [1], ELSA [2] and ESRF (GRAAL) [3,4], had allowed to establish that the η photoproduction reaction mechanism was dominated by the $S_{11}(1535)$ excitation, while the $D_{13}(1520)$ played a small but non-negligible role [5–11]. The measurements for polarization observables also made it possible to single out the contribution of the $F_{15}(1680)$ resonance [8]. However, detailed properties concerning the ηNN^* couplings and even the ηNN coupling still could not be well-constrained at that time, including the total decay width of the dominant $S_{11}(1535)$, and its branching ratio into ηN . Such a situation somehow stalked theoretical progresses due to lack of constrained inputs for the modellings, although various QCD inspired phenomenologies, such as the quark model approaches [6,12–14,8], and formalisms based on the meson-nucleon degrees of freedom using isobaric descriptions [7,9,11], or multipole analyses [5,10], were proposed to investigate the roles played by the intermediate resonances in the η photoproduction.

The situation was changed significantly with the electroproduction data available from JLab [15], which brought rich complementary information about the $S_{11}(1535)$ properties and the D -wave influences, due to the presence of the longitudinal photon excitations. Such an observable is not only valuable for model-selection, but also useful for disentangling

model-dependent or model-independent aspects within a phenomenology.

In this paper, we shall study the η meson electroproduction in a constituent quark model with a chiral effective Lagrangian for the quark-meson (η) couplings, and focus our attentions on the dominant $S_{11}(1535)$ and $D_{13}(1520)$ resonance. The formalism is discussed in Sec. II. In Sec. III, we present detailed results produced by our model fits. This will allow us to proceed to a successful constraint on the $S_{11}(1535)$ properties. The conclusions are given in Sec. IV.

II. THEORETICAL FRAME

In this work, we follow the scheme of a recently developed quark model approach to the pseudoscalar meson photoproduction [12], and extend it to the η meson electroproduction in the region of the c.m. energy $W = 1.535$ GeV. Compared to an isobaric approach, in this model the intermediate baryon resonances can be systematically included in the formalism. Starting from the NRCQM [16], only a limited number of adjustable parameters will appear in the model.

A. Formalism

For the meson interaction vertex, a QCD inspired effective Lagrangian [17] is introduced to account for the quark-meson interaction:

$$L_{eff} = \sum_j \frac{1}{f_\eta} \bar{\psi}_j \gamma_\mu^j \gamma_5^j \psi_j \partial^\mu \phi_\eta , \quad (1)$$

where ψ_j ($\bar{\psi}_j$) is the j th quark (anti-quark) field in the nucleon, and ϕ_η represents the η meson field. At quark level, the transition matrix element \mathcal{M}_{fi} can be expressed as the sum over the t -, s - and u -channel transitions, i.e. $\mathcal{M}_{fi} = \mathcal{M}_{fi}^t + \mathcal{M}_{fi}^s + \mathcal{M}_{fi}^u$. Since \mathcal{M}_{fi}^t is proportional to the charge of the outgoing meson, it vanishes in the neutral meson production. In the s - and u -channel, contributions from a complete set of intermediate baryon resonances are included in the quark model $SU(6) \otimes O(3)$ symmetry limit. It can be seen easily that due to the

isospin conservation, isospin 3/2 states cannot contribute in this channel. Nevertheless, the Moorhouse selection rule eliminates the states of representation [70, 48] from contributing to the proton target reaction [18]. Thus, eight isospin-1/2 resonances corresponding to the harmonic oscillator quantum numbers $n=1$ and 2, and the nucleon pole terms, are to be included explicitly. States with $n \geq 2$ are treated as degenerate in the quantum number n .

Adopting Lorentz gauge $k_\mu A^\mu = 0$, the longitudinal virtual photon polarization vector is defined as

$$\varepsilon_\mu^L = \frac{1}{\sqrt{Q^2}} (|\mathbf{k}|, 0, 0, \omega_\gamma) , \quad (2)$$

where $|\mathbf{k}|$ and ω_γ are the momentum and energy of the virtual photon in the meson-nucleon c.m. frame, respectively. Gauge invariance requires that the longitudinal transition operator is proportional to $\sqrt{Q^2}/|\mathbf{k}|$. Therefore, the longitudinal transition vanishes in the real photon limit. The longitudinal electromagnetic interaction is defined as

$$H_{em}^L = \varepsilon_0^L J_0 - \varepsilon_3^L J_3 , \quad (3)$$

where the electromagnetic current components J_0 and J_3 for a three-quark system can be expressed as

$$J_0 = \sqrt{4\pi} \frac{1}{\sqrt{2\omega_\gamma}} \sum_{j=1}^3 e_j e^{i\mathbf{k}\cdot\mathbf{r}_j} , \quad (4)$$

and

$$J_3 = \sqrt{4\pi} \frac{1}{\sqrt{2\omega_\gamma}} \sum_{j=1}^3 e_j \alpha_j e^{i\mathbf{k}\cdot\mathbf{r}_j} , \quad (5)$$

with e_j denotes the charge operator of the j th quark, and α_j , the Dirac matrix. Given the Hamiltonian of the three-quark system described by only two-body interactions [19], the current conservation gives

$$\langle N_f | J_3 | N_i \rangle = \frac{E_f - E_i}{k_3} \langle N_f | J_0 | N_i \rangle , \quad (6)$$

where $k_3 = |\mathbf{k}|$ and the energy conservation gives $E_f - E_i = \omega_\gamma$. The longitudinal interaction can then be written as

$$H_{em}^L = \left[\varepsilon_0^L - \varepsilon_3^L \frac{\omega_\gamma}{k_3} \right] J_0 . \quad (7)$$

Substituting the ε_μ^L into the above equation, one obtains the gauge-invariant relation:

$$\langle N_f | H_{em}^L | N_i \rangle = \sum_{j=1}^3 \frac{\sqrt{Q^2}}{|\mathbf{k}|} \langle N_f | J_0 | N_i \rangle . \quad (8)$$

We adopt the following nonrelativistic expansion of J_0 for the longitudinal transition [20]:

$$J_0^{NR} = \sqrt{4\pi} \frac{1}{\sqrt{2\omega_\gamma}} \left\{ \sum_j \left[e_j + \frac{ie_j}{4m_j^2} \mathbf{k} \cdot (\boldsymbol{\sigma}_j \times \mathbf{p}_j) \right] e^{i\mathbf{k} \cdot \mathbf{r}_j} - \sum_{j < l} \frac{i}{4M_T} \left(\frac{\boldsymbol{\sigma}_j}{m_j} - \frac{\boldsymbol{\sigma}_l}{m_l} \right) \cdot \left[e_j \mathbf{k} \times \mathbf{p}_l e^{i\mathbf{k} \cdot \mathbf{r}_j} - e_l \mathbf{k} \times \mathbf{p}_j e^{i\mathbf{k} \cdot \mathbf{r}_l} \right] \right\} , \quad (9)$$

where the first term describes the c.m. motion of the three-quark system and is commonly used in the longitudinal transitions. The second and third terms are spin-orbit and non-additive terms, which are believed to be the leading order relativistic corrections to the transition operators [21]. We shall neglect the spin-orbit and non-additive terms in this work. It can be seen later that this approximation will result in an over-estimation of the $S_{11}(1535)$ longitudinal excitation cross section. Empirically, a coefficient for the S_{11} longitudinal transition amplitude will be introduced.

The transverse transition amplitude for the photoproduction have been derived in Ref. [12], in which the transition amplitudes for the $S_{11}(1535)$ and $D_{13}(1520)$ are

$$\mathcal{M}_{S_{11}} = \frac{2M_{S_{11}} e^{-\frac{\mathbf{k}^2 + \mathbf{q}^2}{6\alpha^2}}}{(s - M_{S_{11}}^2 + iM_{S_{11}}\Gamma_{S_{11}})} \frac{1}{6} \left(\frac{\omega_\eta}{\mu_q} - \left(\frac{\omega_\eta}{E_f + M_N} + 1 \right) \frac{2\mathbf{q}^2}{3\alpha^2} \right) \left(\omega_\gamma + \frac{\mathbf{k}^2}{2m_q} \right) \boldsymbol{\sigma} \cdot \boldsymbol{\epsilon}_\gamma , \quad (10)$$

and

$$\begin{aligned} \mathcal{M}_{D_{13}} = & \frac{2M_{D_{13}} e^{-\frac{\mathbf{k}^2 + \mathbf{q}^2}{6\alpha^2}}}{(s - M_{D_{13}}^2 + iM_{D_{13}}\Gamma_{D_{13}})} \left\{ \left(\frac{\omega_\eta}{E_f + M_N} + 1 \right) \frac{\mathbf{q}^2}{9\alpha^2} \left(\omega_\gamma + \frac{\mathbf{k}^2}{2m_q} \right) \boldsymbol{\sigma} \cdot \boldsymbol{\epsilon}_\gamma \right. \\ & - \frac{i}{2m_q} \left(\frac{\omega_\eta}{E_f + M_N} + 1 \right) \frac{\mathbf{k} \cdot \mathbf{q}}{3\alpha^2} \boldsymbol{\sigma} \cdot \mathbf{q} \boldsymbol{\sigma} \cdot (\mathbf{k} \times \boldsymbol{\epsilon}_\gamma) \\ & \left. - \left(\frac{\omega_\eta}{E_f + M_N} + 1 \right) \frac{\omega_\gamma}{3\alpha^2} \boldsymbol{\sigma} \cdot \mathbf{q} \boldsymbol{\epsilon}_\gamma \cdot \mathbf{q} \right\} , \quad (11) \end{aligned}$$

where μ_q is the reduced mass of two quarks and equals $m_q/2$ in the η production for $m_u = m_d = m_q$. The overall coupling α_η is related to the η meson radiative decay constant f_η by assuming the validity of the Goldberger-Treiman relation [22] for the ηNN couplings:

$$g_{\eta NN} = \frac{g_A M_N}{f_\eta}, \quad (12)$$

with $\alpha_\eta \equiv g_{\eta NN}^2/4\pi$, where $g_A = 1$ is given by the NRCQM in the $SU(6)\otimes O(3)$ symmetry limit.

Similarly, the amplitudes for other resonances in the quark model can be derived. In this paper, we concentrate on the kinematics from threshold to $W \sim 1.54$ GeV, where the available experimental data allow a close study of the $S_{11}(1535)$ and $D_{13}(1520)$. One of the advantages is that one can neglect the $SU(6)\otimes O(3)$ symmetry violations for other excited states. Therefore, we could only introduce an $SU(6)\otimes O(3)$ breaking coefficient for the $S_{11}(1535)$ and $D_{13}(1520)$. In another word, except for the $S_{11}(1535)$ and $D_{13}(1520)$, the relative strengths among other resonances will be constrained by the quark model. In this way, we avoid to introduce too many parameters in the model. This treatment is different from that in Refs. [8] and [23]. Another feature in this calculation is that the quark model parameters are also taken into account. The harmonic oscillator strength α is treated as a free parameter, of which a value within the range of quark model validity could be an essential test of the self-consistence of this model. Moreover, the $S_{11}(1535)$ total width $\Gamma_{S_{11}}$ and its partial decay branching ratio b_η into ηN will be treated as free parameters as well.

B. Kinematics and observables

The kinematics of the meson exclusive electroproduction has been discussed in the literature [24,25]. Here, we directly relate the kinematics to our convention of the transition amplitude. Generally, the cross section of the meson electroproduction can be written as follows:

$$\frac{d\sigma}{dE'_e d\Omega_2 d\Omega^*} = \Gamma_v \frac{d\sigma}{d\Omega^*}, \quad (13)$$

where, $d\sigma/d\Omega^*$ represents the cross section for the virtual-photon-nucleon scattering in the meson-nucleon c.m. frame, while the contribution from the lepton current can be factorized into a factor Γ_v which is known as the virtual photon flux

$$\Gamma_v = \frac{\alpha_e E'_e K_E}{2\pi^2 E_e Q^2} \frac{1}{1 - \varepsilon} , \quad (14)$$

where α_e is the electromagnetic fine structure constant, E_e and E'_e are the energies of the initial and scattered electrons, respectively, in the lab system, and $K_E = (s - M^2)/2M$ is the equivalent energy of the virtual photon as a real photon in the lab system.

The virtual photon polarization parameter, ε , is defined as

$$\varepsilon = (1 + 2 \tan^2(\frac{\theta_e}{2}) |\mathbf{k}_0|^2 / Q^2)^{-1} . \quad (15)$$

where \mathbf{k}_0 is the virtual photon momentum in the lab system.

The cross section for the meson production by the virtual photon in the meson-nucleon c.m. frame can be expressed as

$$\frac{d\sigma}{d\Omega^*} = \frac{d\sigma_T}{d\Omega^*} + \varepsilon \frac{d\sigma_L}{d\Omega^*} - \varepsilon \frac{d\sigma_{TT}}{d\Omega^*} \cos 2\phi_\eta^* - \sqrt{\varepsilon(1 + \varepsilon)} \frac{d\sigma_{TL}}{d\Omega^*} \cos \phi_\eta^* , \quad (16)$$

where ϕ_η^* is the azimuthal angle between the ηN scattering plane and the (e, e') scattering plane, and

$$\frac{d\sigma_T}{d\Omega^*} = \xi \frac{2|\mathbf{k}|^2}{Q^2} \mathcal{H}^{00} , \quad (17)$$

$$\frac{d\sigma_L}{d\Omega^*} = \xi (\mathcal{H}^{11} - \mathcal{H}^{-1-1}) , \quad (18)$$

$$\frac{d\sigma_{TT}}{d\Omega^*} = \xi (\mathcal{H}^{1-1} + \mathcal{H}^{-11}) , \quad (19)$$

$$\frac{d\sigma_{TL}}{d\Omega^*} = \xi \sqrt{\frac{|\mathbf{k}|^2}{Q^2}} (\mathcal{H}^{01} + \mathcal{H}^{10} - \mathcal{H}^{0-1} - \mathcal{H}^{-10}) . \quad (20)$$

In the above equations, ξ represents the phase space factor in the virtual-photon-nucleon excitations, and has the following expression:

$$\xi = \frac{\alpha_e M_N |\mathbf{q}|}{16\pi W K_E} , \quad (21)$$

where $|\mathbf{q}| = [(s - M_N^2 - m_\eta^2)^2 - 4M_N^2 m_\eta^2]^{\frac{1}{2}} / (2W)$ is the meson momentum in the meson-nucleon c.m. frame. The amplitude, $\mathcal{H}^{\lambda\lambda'}$, is defined as

$$\mathcal{H}^{\lambda\lambda'} = \sum_{\lambda_1 \lambda_2} \mathcal{A}_{\lambda_1 \lambda_2}^\lambda \mathcal{A}_{\lambda_1 \lambda_2}^{\lambda' \dagger} , \quad (22)$$

where $\mathcal{A}_{\lambda_1\lambda_2}^\lambda$ are the transition amplitudes for the meson production via the virtual photon, $\lambda = 0, \pm 1$ denotes the spin polarizations of the incoming virtual photon and, $\lambda_1 = \pm\frac{1}{2}$ and $\lambda_2 = \pm\frac{1}{2}$ for the initial and final state nucleons, respectively. In the pseudoscalar meson electroproduction, there are two independent amplitudes in the longitudinal photon transitions, and four independent amplitudes in the transverse photon transitions. The latter ones can be related to the traditional CGLN amplitudes or the helicity amplitudes [26].

When the calculations are extended to the electroproduction, it becomes highly relativistic, and a Lorentz boost factor must be introduced into the spatial integrals. We follow the prescription of Foster and Hughes [27] to boost momentum for the spatial integrals in an equal velocity frame (EVF), which is very close to the Breit frame. In the EVF, the Lorentz boost factor for the virtual photon interaction is defined as

$$\gamma_k = \left(1 + \frac{k^2}{(W + M_N)^2}\right)^{\frac{1}{2}}, \quad (23)$$

where the relation of the momentum k with the Q^2 in the EVF is

$$k^2(EVF) = \frac{(W^2 - M_N^2)^2}{4WM_N} + \frac{Q^2(W + M_N)^2}{4WM_N}. \quad (24)$$

With the boost factor, the spatial integral concerning the photon excitation is boosted as

$$R(k) \rightarrow \frac{1}{\gamma_k^2} R\left(\frac{k}{\gamma_k}\right). \quad (25)$$

The same prescription can be adopted for the resonances decaying into the final state η meson and proton:

$$\gamma_q = \left(1 + \frac{q^2}{(W + M_N)^2}\right)^{\frac{1}{2}}, \quad (26)$$

where

$$q^2(EVF) = \frac{(W^2 - M_N^2)^2}{4WM_N} - \frac{m_\eta^2(W + M_N)^2}{4WM_N}. \quad (27)$$

Therefore, the spatial integrals in the transition matrix elements from the initial states to the final states can be expressed as

$$R(k, q) \rightarrow \frac{1}{\gamma_k^2} \frac{1}{\gamma_q^2} R\left(\frac{k}{\gamma_k}, \frac{q}{\gamma_q}\right). \quad (28)$$

Compared to the previous study of the η meson photoproduction [8], in which the Lorentz boost factors, $\gamma_k = E_i/M_N$ and $\gamma_q = E_f/M_f$, in the c.m. frame of the meson-nucleon system were adopted, the Lorentz boost factors in the EVF turn out to be more successful in reproducing the data. The failure of the Lorentz boost factor γ_k in the meson-nucleon c.m. frame can be seen more clearly by rewriting it in the electroproduction:

$$\frac{1}{\gamma_k^2} = \left(\frac{M_N}{E_i}\right)^2 = \frac{4sM_N^2}{(s + M_N^2)^2} \frac{1}{(1 + Q^2/(s + M_N^2))^2}. \quad (29)$$

Since $4sM_N^2/(s + M_N^2)^2 \leq 1$, the rest part plays a role as a dipole in the nucleon's electromagnetic form factor. Note that, the c.m. energy $W \equiv \sqrt{s}$ is fixed at $M_{S_{11}}$, therefore, $(s + M_N^2)$ is a constant. In contrast to the Lorentz boost factor in the EVF, an *ad hoc* dipole, $1/(1 + Q^2/0.71)^2$, was widely used for the nucleon's electromagnetic form factor in the literature [28]. Such a Q^2 -dependence results in a fast drop-down behavior, which underestimates the data significantly at high Q^2 regions.

To show the difference between the two Lorentz boost schemes, we present the Q^2 -dependence of the $1/\gamma_k^2$ factor calculated at $W = 1.535$ GeV by Eqs. 23 (solid curve) and 29 (dashed curve) in Fig. 1. It shows that in the EVF, electromagnetic transition is boosted rather moderately than in the meson-nucleon c.m. frame. The difference between these two frames reveals non-covariance of this approach. As the boost goes large, a more realistic prescription is needed.

For the meson interaction vertex, the boost factor at $W = 1.535$ GeV in both frames is a constant, and possesses very close values, i.e., $1/\gamma_q^2 = 0.99$ in the EVF and 0.96 in the meson-nucleon c.m. frame. Such a feature is due to the quite heavy mass of the η meson and its relatively small on-mass-shell momentum.

III. RESULTS AND DISCUSSIONS

In this Section, we present numerical results for various photo- and electroproduction observables. Parameters are fitted by experimental data. Meanwhile, an analytical relation is deduced in the study of the $S_{11}(1535)$ excitations.

A. Database and adjustable parameters

The newly published data [15] cover the kinematics $1.490 \leq W \leq 1.615$ GeV at $Q^2 = 2.4$ and 3.6 (GeV/c)², have greatly improved the experimental status of the η meson photo- and electroproduction. Along with three other datum sets: old electroproduction data at $W=1.535$ GeV with $Q^2 = 0.20, 0.28$ and 0.40 (GeV/c)² [29], and recent photoproduction cross section data from Mainz [1] and GRAAL [4] from ηN threshold to $E_\gamma^{lab} \leq 0.9$ GeV (corresponding to $W = 1.6$ GeV), we obtain a large database covering the complete kinematics of the $S_{11}(1535)$ and $D_{13}(1520)$ excitations. This opportunity will allow us to concentrate on these two resonances, whose couplings to the ηN channel have not been well known. Note that, the Mainz data cover the energy range from threshold to $E_\gamma^{lab}=0.789$ GeV, while the GRAAL data go to higher energies: $0.714 < E_\gamma^{lab} \leq 1.1$ GeV. For GRAAL data we use a subset restricted to $E_\gamma^{lab} \leq 0.9$ GeV.

The complete database contains 677 differential cross-sections and has been used to fix 7 adjustable parameters in this approach. The results, obtained using the CERN MINUIT minimization code, are given in Table I. Below, we summarize the main features of each parameters based on the numerical investigations.

The ηNN coupling constant ($\alpha_\eta \equiv g_{\eta NN}^2/4\pi$) is not a well-determined quantity in the literatures. Here, α_η is an overall factor and the numerical fits give $\alpha_\eta = 0.10 \pm 0.01$. Recent studies [8,30,31] suggest that $g_{\eta NN}^2/4\pi$ is much smaller than unit.

The commonly used value for the second free parameter, namely, the harmonic oscillator strength α varies between 330 and 430 MeV in the literatures. In the numerical fitting,

a rather moderate value, $\alpha = 384.5$ MeV, is extracted. With the quark model spatial wavefunctions boosted in the EVF, Such a value avoids the introduction of an *ad hoc* dipole or monopole in the form factor ¹. Then, the exponential factor from the spatial integrals, $e^{-(\mathbf{k}^2+\mathbf{q}^2)/6\alpha^2}$, will play a role like a form factor after being boosted.

The $S_{11}(1535)$'s total width $\Gamma_{S_{11}}$ and its ηN decay branching ratio b_η have been very important in the study of its nature. However, both experimental values and theoretical predictions for these two quantities have been very contradictory in the literatures [1,15,32,33]. The η meson photo- and electroproduction at the S_{11} mass region show great sensitivities to these two quantities. Much stronger constraints from the electroproduction data are found in this calculation. Treating the two quantities as free parameters, we extract $\Gamma_{S_{11}} = 143.3 \pm 0.2$ MeV and $b_\eta(S_{11}) = 0.55 \pm 0.01$. These results are very close to the most recent extraction from the JLab data [15]. For other resonances, their total widths and partial decay branching ratios are found not to be sensitive in this kinematical region. Therefore, we use the total widths from the Particle Data Group (PDG) [34] in the calculation. The partial decay channels for those resonances are restricted to the πN and ηN , with branching ratios fixed at $b_\pi=90\%$ and $b_\eta=10\%$. As a sensitivity test, we also use $b_\pi=99\%$ and $b_\eta=1\%$ and found that the numerical results do not show significant dependence on these branching ratios due to the dominance of the $S_{11}(1535)$.

The fifth and sixth parameter, $C_{S_{11}}$ and $C_{D_{13}}$, are strength coefficients introduced for the $S_{11}(1535)$ and $D_{13}(1520)$ amplitudes to take care of the breaking of the $SU(6) \otimes O(3)$ symmetry. As discussed in Sec. II, eight resonances with harmonic oscillator shell $n \leq 2$ are to be

¹ In Ref. [27], the authors adopted a larger value for the harmonic oscillator strength, $\alpha = 458.2$ MeV. Meanwhile, a monopole form factor, $F_q(Q^2) = 1/(1 + Q^2/0.8)$, had to be adopted to produce the dying-out behavior of the resonance helicity amplitudes in the Q^2 -dependence. Also, it was shown that a smaller value $\alpha = 331.7$ MeV with $F_q(Q^2) = 1$ could nicely reproduce the helicity amplitudes for the $S_{11}(1535)$. See the dot-dashed curve in Fig. 1c of Ref. [27].

explicitly included, i.e., $S_{11}(1535)$, $D_{13}(1520)$, $P_{13}(1720)$, $F_{15}(1680)$, $P_{11}(1440)$, $P_{11}(1710)$, $P_{13}(1900)$, and $F_{15}(2000)$. In the $SU(6)\otimes O(3)$ symmetry limit, the relative strengths of all these resonances and higher mass terms are fixed with the same quark-meson coupling denoted by α_η , apart from the quark model couplings. The configuration mixing among excited states, which breaks the $SU(6)\otimes O(3)$ symmetry, in principle should be taken into account. However, since the complexity arising from such a scheme somehow cannot be easily controlled, one can take an empirical strategy to introduce the strength coefficient C_{N^*} for each resonance [8,23]. These coefficients can be determined by numerical fits, and their deviations from unit will reflect the breaking of the $SU(6)\otimes O(3)$ symmetry. In this study, the selected kinematical region allows us to focus on the two resonances $S_{11}(1535)$ and $D_{13}(1520)$. Thus, only $C_{S_{11}}$ and $C_{D_{13}}$ are introduced and treated as parameters. It should be noted that, coefficients $C_{S_{11}}$ and $C_{D_{13}}$ were found close to unit in a recent photoproduction study [23].

Finally, we include an additional coefficient $C_{S_{11}}^L$ for the the longitudinal excitation amplitude of the S_{11} in the electroproduction process. This quantity will be discussed in the following Section with respect to the experimental indications [35,36].

B. Analysis of observables

With those parameters (Table I) extracted in the data fits, we shall proceed to the detailed analyses of the model-fitting results. Predictions thus can be made for various observables. Some dynamical features arising from the electroproduction processes will be investigated. The $S_{11}(1535)$ properties can be reasonably constrained.

1. Cross-sections

In Fig. 2, the fitting results for the photoproduction process are shown for energies from threshold up to $E_\gamma^{lab} = 900.4$ MeV. The full curves come from the model outlined above and reproduce well enough the data. The dashed curve in Fig. 2 at $E_\gamma = 790$ MeV denotes the

result in the absence of the $D_{13}(1520)$ contribution at the $S_{11}(1535)$ energy. Comparison between the full and dashed curve shows that the $D_{13}(1520)$ plays a small but non-negligible role in $\gamma p \rightarrow \eta p$. It accounts for the main non- S -wave behavior in the angular distributions. Meanwhile, the S_{11} dominance is displayed by the (almost) isotropic behavior of the dashed curve.

In Fig. 3, the differential cross sections for the electroproduction process at low- Q^2 are presented (full curve) and compared with the old data at $Q^2 = 0.4$ (GeV/c)² with $\varepsilon = 0.79$ and $\phi_\eta^* = 0^\circ$ [29]. Components of the cross section (Eq. 16) are also presented: transverse (dashed curve), longitudinal (dotted curve), transverse-transverse (TT) interfering (dash-dotted), and transverse-longitudinal (TL) interfering component (heavy dotted curve). Since the longitudinal contribution is quite small, it is the TT interference that accounts for the structure at small angles as shown by the solid curve. Meanwhile, it shows that the data prefer even smaller longitudinal cross sections at this region, although the fits are in agreement with the data reasonably.

The recent precise measurements [15] of the η meson electroproduction at $Q^2 = 2.4$ and 3.6 (GeV/c)² are successfully fitted by this approach. In Fig. 4, the angular distributions at $W = 1.54$ GeV with different azimuthal angles ϕ_η^* for both momentum transfers are presented. The polarization parameters are $\varepsilon = 0.51$ for $Q^2 = 2.4$ (GeV/c)² and 0.46 for $Q^2 = 3.6$ (GeV/c)². The solid curves represent the results for $Q^2 = 3.6$ (GeV/c)² and the dashed curves for $Q^2 = 2.4$ (GeV/c)². The results in the absence of the $D_{13}(1520)$ at $Q^2 = 3.6$ (GeV/c)² are shown by the dotted curves. It confirms that the non- S -wave feature of the data is due to the $D_{13}(1520)$ interference. Meanwhile, other resonances and the nucleon pole terms have only negligible influences. At $Q^2 = 3.6$ (GeV/c)², the fits start to underestimate the experimental dots. It might suggest that the NRCQM form factor for the $D_{13}(1520)$ becomes inappropriate with the increasing Q^2 . In Ref. [37], the data showed that the D_{13} form factor had more steeper slope with the increasing Q^2 , which led to a negligible D_{13} contribution above $Q^2 = 3.0$ (GeV/c)². However, in Fig. 4, the D_{13} still makes sense at $Q^2 = 3.6$ (GeV/c)², which means it does not decrease as fast as the data

would require.

With the parameters fixed, in Fig. 5, the Q^2 -dependence of the transverse and longitudinal components of the total cross section are shown by the dashed and dotted curves, respectively. We plot the total cross section $\sigma_{tot} = \sigma_T + \varepsilon\sigma_L$ (full curve), at the $W = 1.535$ GeV, with $\varepsilon=0.6$. The value of the latter quantity corresponds to the JLab experiment kinematics [15]. The data are correctly reproduced. Although the values of ε , determined by the experimental kinematics, varies from one datum set to another, the chosen value for ε is not crucial in the illustration of the calculation. This is due to the fact that σ_L comes out much smaller than σ_T .

An interesting quantity to be investigated is the ratio $R(Q^2) = \sigma_L/\sigma_T$. Its Q^2 -dependence was found to be quite smooth in both experiment [35,36,38] and theory [28].

As a preparation, the two well known relations for an excited resonance in $\gamma_{(v)}N \rightarrow \eta N$ are presented:

$$\sigma_T = \frac{M_N}{M_R} \frac{b_\eta}{\Gamma_R} 2\{|A_{\frac{1}{2}}|^2 + |A_{\frac{3}{2}}|^2\} , \quad (30)$$

and

$$\sigma_L = \frac{Q^2}{|\mathbf{k}|^2} \frac{M_N}{M_R} \frac{b_\eta}{\Gamma_R} 4|S_{\frac{1}{2}}|^2 , \quad (31)$$

where, Γ_R is the total width of the resonance and $b_\eta \equiv \Gamma_\eta/\Gamma_R$ is the branching ratio of the resonance decaying into ηN .

In the calculations, we find that the inclusive (all contributions) and exclusive (only S_{11}) cross sections produce the same ratios because the S_{11} dominates in both σ_L and σ_T . Then, the ratio can be expressed as

$$R_{th}(Q^2) \equiv \frac{\sigma_L}{\sigma_T} \approx \frac{2Q^2}{|\mathbf{k}|^2} \frac{|S_{\frac{1}{2}}|^2}{|A_{\frac{1}{2}}|^2} . \quad (32)$$

Note that, the amplitude $A_{\frac{3}{2}}$ vanishes in the S_{11} excitations.

However, in both inclusive and exclusive calculations, the present NRCQM study slightly overestimates the experimental result [35]. Empirically, we define a parameter $C_{S_{11}}^L$ for the S_{11} longitudinal amplitude such that

$$R_{exp}(Q^2) \equiv (C_{S_{11}}^L)^2 R_{th}(Q^2) . \quad (33)$$

Given $R_{exp} = 0.23 \pm 0.11$ at $Q^2 = 0.4$ (GeV/c)² from Ref. [35], we find $C_{S_{11}}^L = (R_{exp}/R_{th})^{\frac{1}{2}} = 0.70$. This result is in good agreement with the fitted value $C_{S_{11}}^L = 0.65$ in Table I, and explains the introduction of this parameter for the S_{11} . The successful extraction of $C_{S_{11}}^L$ in the fits suggests that the leading order relativistic correction to the $S_{\frac{1}{2}}$ could be absorbed into the parameter $C_{S_{11}}^L$ and such a correction might not be sensitive to a wide Q^2 range. The latter point can be explained by the flat Q^2 dependence of the ratio. In Fig. 6, the ratio $R_{th}(Q^2) \equiv \sigma_L/\sigma_T$ is calculated using different values for $C_{S_{11}}^L$. The solid curve denotes the result for $C_{S_{11}}^L = 0.65$, the dashed for $C_{S_{11}}^L = 1$, and the dotted for $C_{S_{11}}^L = 0.70$. The maximum ratio is at $Q^2 \approx 0.5$ (GeV/c)², which is in agreement with the finding of Ref. [28].

In the following part, we will see that the overestimation of the longitudinal cross section σ_L comes mainly from the photon vertex, where the longitudinal helicity amplitude $S_{\frac{1}{2}}$ has been overestimated.

2. $S_{11}(1535)$ photo- and electro-excitation helicity amplitudes

To better understand the overestimation of the σ_L , we independently calculate $S_{\frac{1}{2}}$ of the transition $\gamma_{(v)}p \rightarrow S_{11}(1535)$ in the EVF,

$$S_{\frac{1}{2}} = \frac{1}{3} \sqrt{\frac{\pi}{\omega_\gamma}} \alpha_e^{\frac{1}{2}} \frac{|\mathbf{k}|}{\alpha \gamma_k^3} e^{-\frac{\mathbf{k}^2}{6\alpha^2 \gamma_k^2}} , \quad (34)$$

where $1/\gamma_k$ is the Lorentz boost factor defined in previous Section.

On the other hand, we explicitly write out the longitudinal cross section $\sigma_L(S_{11})$ for the $S_{11}(1535)$,

$$\sigma_L(S_{11}) = \frac{Q^2}{|\mathbf{k}|^2} \frac{\pi}{\omega_\gamma} \frac{\alpha_e \alpha_{S_{11}} |\mathbf{q}| |\mathbf{k}|^2}{M_N M_{S_{11}} \Gamma_{S_{11}}^2} \frac{8}{9} \left[\frac{\omega_\eta}{\mu_q} - \left(\frac{\omega_\eta}{E_f + M_N} + 1 \right) \frac{2\mathbf{q}^2}{3\alpha^2 \gamma_q} \right]^2 \frac{e^{-(\mathbf{k}^2/\gamma_k^2 + \mathbf{q}^2/\gamma_q^2)/3\alpha^2}}{\gamma_q^4 \gamma_k^6} , \quad (35)$$

where the Lorentz boost factors have been included and the kinematical condition $s = M_{S_{11}}^2$ at the $S_{11}(1535)$ c.m. energy has been used. Substituting the above equation into Eq. 31, $S_{\frac{1}{2}}$ can be also derived:

$$|S_{\frac{1}{2}}|^2 = (C_{S_{11}}^L)^2 \frac{\pi}{\omega_\gamma} \frac{\alpha_e \alpha_{S_{11}} |\mathbf{q}| |\mathbf{k}|^2}{M_N^2 b_\eta \Gamma_{S_{11}}} \frac{2}{9} \left[\frac{\omega_\eta}{\mu_q} - \left(\frac{\omega_\eta}{E_f + M_N} + 1 \right) \frac{2\mathbf{q}^2}{3\alpha^2 \gamma_q} \right]^2 \frac{e^{-(\mathbf{k}^2/\gamma_k^2 + \mathbf{q}^2/\gamma_q^2)/3\alpha^2}}{\gamma_q^4 \gamma_k^6} . \quad (36)$$

In Fig. 7, the results for $S_{\frac{1}{2}}$ from Eq. 34 (dotted curve) and from Eq. 36 with $C_{S_{11}}^L = 0.65$ (solid curve) and $C_{S_{11}}^L = 1$ (dashed curve), are presented. Interestingly, it shows that although the dotted and dashed curves both overestimate the helicity amplitude $S_{\frac{1}{2}}$, their values are very close. We thus equate these two expressions to give:

$$b_\eta = \frac{\alpha_{S_{11}}}{\Gamma_{S_{11}}} \chi , \quad (37)$$

where

$$\chi \equiv \frac{2\alpha^2 |\mathbf{q}|}{M_N^2} \left[\frac{\omega_\eta}{\mu_q} - \left(\frac{\omega_\eta}{E_f + M_N} + 1 \right) \frac{2\mathbf{q}^2}{3\alpha^2 \gamma_q} \right]^2 \frac{e^{-\frac{\mathbf{q}^2}{3\alpha^2 \gamma_q^2}}}{\gamma_q^4} , \quad (38)$$

and $\alpha_{S_{11}} \equiv \alpha_\eta (C_{S_{11}})^2$ is the $\eta p S_{11}$ coupling constant.

Intuitively, the above expression is a reasonable deduction since Eq. 37 is exactly the branching ratio obtained by calculating $S_{11}(1535) \rightarrow \eta p$. However, recalling that b_η and $\Gamma_{S_{11}}$ are quantities to be investigated here, relations (as Eqs. 37-38) derived from only $S_{11}(1535) \rightarrow \eta p$ cannot help us much, not mention that $\alpha_{S_{11}}$ is also unclear. We thus expect that information about these quantities can be derived in the photo- and electroproduction process. Unfortunately, another difficulty arises from the electromagnetic vertex in photo- and electroproduction. Since the experiment cannot separate the $\gamma N S_{11}$ from the strong $\eta N S_{11}$ couplong, studies of $\gamma N \rightarrow S_{11}$ and $S_{11} \rightarrow \eta N$ are strongly model-dependent [21]. Therefore, the fit of the photo- and electroproduction data generally tells us what is the ‘‘parameter’’ (e.g. $\alpha_{S_{11}}$) for $\gamma N \rightarrow S_{11} \rightarrow \eta N$ instead of what is the coupling for $S_{11} \rightarrow \eta N$. The overestimation of the $S_{\frac{1}{2}}$ is an example exposing this kind of problems.

Now, the trivial-look Eqs. 37 and 38 can tell us more about the $\eta N S_{11}$ coupling. First, since these quantities, b_η , $\Gamma_{S_{11}}$, and $\alpha_{S_{11}}$, are determined by fitting the reaction, we thus should bear in mind that their values have contained uncertainties from the electromagnetic interactions. Also, the model-dependent feature arising from non- S_{11} contributions could mix into the fitted values for those parameters. As shown by Fig. 7, although the fitted

quantity $C_{S_{11}}^L = 0.65$ better accounts for the data, we obviously cannot equate the solid curve to the dotted one. In that case, Equations 37 and 38 would not be a natural deduction at all. The non-trivial thing occurs only if we take all parameters fitted by the data except for $C_{S_{11}}^L = 1$ to produce the dashed curve in Fig. 7. Namely, both overestimations of the electromagnetic coupling turn to be equal to each other. Thus, it leads to the relation of Eq. 37, in which the electromagnetic coupling has been cleanly removed. Since on the one hand, no information about the electromagnetic interaction is contained in Eqs. 37 and 38 any more, and on the other hand, all quantities involved are determined by the fits, these two equations in effect provide an additional relation for all those fitted quantities. We thus can ask the question concerning the self-consistence of the model fitting results, *whether those quantities fitted by the reaction data can satisfy the relation?* Again, we have to bear in mind that those quantities could have contained all uncertainties arising from the electromagnetic coupling as well as model-dependent features from the non- S_{11} terms.

To answer the question, we calculate the partial decay width of the $S_{11}(1535)$ using those fitted quantities, i.e. $\Gamma_\eta^a \equiv b_\eta \Gamma_{S_{11}}$, and $\Gamma_\eta^b \equiv \alpha_{S_{11}} \chi$, where χ is calculated by Eq. 38. The results are presented in Table II. The PDG [34] estimations are also presented. It shows that Γ_η^a and Γ_η^b are in good agreement with each other, although discrepancies also exist. Quite clearly, the discrepancies reveal the uncertainties arising from the model-dependent aspects in the fits, while the consistencies highlight a reasonable constraint to the strong coupling. It suggests that the effective Lagrangian successfully accounts for the $\eta N S_{11}$ coupling within an accuracy of 15%. We shall see below that this conclusion is important for the assessment of the S_{11} transverse helicity amplitude derived in the reaction. Note that the harmonic oscillator strength α has a moderate value 384.5 MeV, which is within the range of commonly used values, 330-430 MeV, this provides another justification for this approach. In this sense, the relation of Eq. 37 could be regarded as being “satisfied” rather than “fitted”.

In the following part, we turn to the results for the transverse helicity amplitude for the $S_{11}(1535)$. From Eq. 30, the transverse helicity amplitude for the $S_{11}(1535)$ can be expressed

as

$$\begin{aligned}
|A_{\frac{1}{2}}|^2 &= \frac{M_{S_{11}} \Gamma_{S_{11}}}{2M_N b_\eta} \sigma_T(\gamma_{(v)}p \rightarrow S_{11} \rightarrow \eta p) \\
&= \frac{\pi \alpha_e \alpha_{S_{11}} |\mathbf{q}| (E_f + M_N)}{\omega_\gamma M_N^2 b_\eta \Gamma_{S_{11}} 2M_N} \\
&\quad \times \left(\omega_\gamma + \frac{\mathbf{k}^2}{2m_q \gamma_k} \right)^2 \frac{e^{-(\mathbf{k}^2/\gamma_k^2 + \mathbf{q}^2/\gamma_q^2)/3\alpha^2}}{\gamma_q^4 \gamma_k^6} \\
&\quad \times \frac{2}{9} \left[\frac{\omega_\eta}{\mu_q} - \left(\frac{\omega_\eta}{E_f + M_N} + 1 \right) \frac{2\mathbf{q}^2}{3\alpha^2 \gamma_q} \right]^2, \tag{39}
\end{aligned}$$

where $\sigma_T(\gamma_{(v)}p \rightarrow S_{11} \rightarrow \eta p)$ is the exclusive transverse cross section calculated by the model, and the Lorentz boost factors are taken into account. The result of Eq. 39 is presented in Fig. 8 (dashed curve), which is in good agreement with the experimental data. It is worth noting that a direct relation as Eq. 37 cannot be obtained for the transverse helicity amplitude. The basic reason is that the EM operators used in this model [12] are essentially different from the NRCQM ones [16]. However, as shown by the dashed curve in Fig. 8, those well constrained parameters indeed provide a reasonable discription of the $S_{11}(1535)$.

Such a result certainly highlights again the relation provided by Eq. 37 and 38. It is also useful for the understanding of a variable defined in the literature. In Ref. [7], it was found that the quantity $\xi_T \equiv \sqrt{\Omega} \Gamma_\eta A_{\frac{1}{2}} / \Gamma_{S_{11}}$, where Ω is the phase space factor, was not sensitive to the fitting scheme since uncertainties within Γ_η and $\Gamma_{S_{11}}$ went to the same direction. That feature arises because the constraint to the $\eta N S_{11}$ vertex was not enough. However, here we find that Eq. 37 restricts the b_η and $\Gamma_{S_{11}}$ in an inverse direction compared to ξ_T . Supposing b_η and $\Gamma_{S_{11}}$ both increase or decrease, the relation of Eq. 37 will be destructively unbalanced. The satisfactory of Eq. 37 thus indeed serves as a further constraint to those fitted quantities.

The dominant $S_{11}(1535)$ production can be investigated by substituting the exclusive $\sigma_T(\gamma_{(v)}p \rightarrow S_{11} \rightarrow \eta p)$ with the inclusive σ_T in Eq. 39:

$$|A_{\frac{1}{2}}|^2 = \frac{M_{S_{11}} \Gamma_{S_{11}}}{2M_N b_\eta} \sigma_T. \tag{40}$$

The difference between Eqs. 39 and 40 reflects the influence of the non- S -wave contributions

in the transverse helicity amplitude. The calculations of Eq. 39 (dashed curve), and Eq. 40 (solid curve) are presented in Fig. 8. It shows that the impact of the non- S_{11} contributions produces about 3% difference in the helicity amplitude, and the transverse cross sections are dominated by the $S_{11}(1535)$ excitation.

In Ref. [15] the impact from the longitudinal cross section have been investigated through the following relation:

$$|A_{\frac{1}{2}}|^2 = \frac{M_{S_{11}} \Gamma_{S_{11}} \sigma_T(\gamma p \rightarrow S_{11} \rightarrow \eta p)}{2M_N b_\eta (1 + \varepsilon R(Q^2))}. \quad (41)$$

As shown in Fig. 5, the ratio $R(Q^2)$ is much smaller than unit, thus, the effect of the longitudinal contribution, reflected by the factor $1/(1 + \varepsilon R(Q^2))$, is found negligible in comparison with Eq. 39, especially at high Q^2 regions.

In Fig. 8, we also present the calculation of $A_{\frac{1}{2}}$ based on the dipole-like Lorentz boost factor in the meson-nucleon c.m. frame (Eq. 29) for the $S_{11}(1535)$ (See the dot-dashed curve). With the same set of parameters, the dot-dashed curve apparently under-estimates the experimental values, although compared to a parametrized dipole form factor, $1/(1 + Q^2/0.8)^2$ (see the dotted curve), it better accounts for the trend of data.

The resonance contributions to the transverse helicity amplitude $A_{\frac{1}{2}}(Q^2)$ drop down with the increasing Q^2 as shown by the full curve in Fig. 8. At high Q^2 region, the pQCD dominance in the helicity-conserved amplitude $A_{\frac{1}{2}}(Q^2)$ predicted the asymptotic behavior of $A_{\frac{1}{2}}(Q^2)$ fall-off like $1/Q^3$ [39]. That is to say, the quantity $Q^3 A_{\frac{1}{2}}(Q^2)$ will approach a constant at high Q^2 regions. However, the studies by Isgur and Smith [42], and Radyushkin [43] led to quite different results. They found that such a scaling behavior in the exclusive processes were still dominated by the non-perturbative contributions rather than the perturbative ones over wide Q^2 regions. We present the calculation of the quantity $Q^3 A_{\frac{1}{2}}(Q^2)$ in Fig. 9 to compare with the data. At $Q^2 = 2.4$ and 3.6 (GeV/c)², the quantity $Q^3 A_{\frac{1}{2}}(Q^2)$ is calculated through Eq. 39. It gives 0.201 and 0.268 GeV ^{$\frac{5}{2}$} , respectively, which are consistent with the non-scaling behavior found in experiment at small Q^2 . At $Q^2 = 4.0$ (GeV/c)², we get $Q^3 A_{\frac{1}{2}} = 0.282$ GeV ^{$\frac{5}{2}$} . This quantity approaches the maximum 0.302 GeV ^{$\frac{5}{2}$} at $Q^2 =$

5.5 (GeV/c)², and then falls down slowly with the increasing Q^2 . However, due to the shortcoming of the NRCQM, the results above 4 (GeV/C)² should not be taken seriously. More fundamental approach is needed for the dying-out region of non-purterbative processes, where a continuing scaling behavior from pQCD processes might emerge.

IV. SUMMARY AND CONCLUSION

This work was motivated by the recent electroproduction data from JLab [15] in the S_{11} dominant kinematical region. We also took advantage of even more recent photoproduction data from GRAAL [4]. Such a database, expected to be significantly enlarged in the near future, offers an excellent opportunity to investigate the reaction mechanism of the η meson photo- and electroproduction. In particular, the selected kinematical region allows us to study the nature of the $S_{11}(1535)$ resonance with unprecedentedly precise data.

The model presented here is an extension of a constituent quark model approach with a chiral effective Lagrangian [12] to the electroproduction process. On the basis of the symmetric NRCQM, there are only a limited number of parameters appearing in this approach. In principle, the breaking of this symmetry can be phenomenologically introduced through an additional coefficient for each resonance, which then could be determined in the numerical study [8,23]. However, different from Refs. [8,23], in this work attentions are paid to the $S_{11}(1535)$ and $D_{13}(1520)$. The selected kinematics permit us to introduce the symmetry breaking coefficients only for the $S_{11}(1535)$ and $D_{13}(1520)$ due to the dominance of the former and significant interferences from the latter. For other resonances, their symmetry breaking coefficients are neglected due to their negligible effects. In this work, the $S_{11}(1535)$'s total width, branching ratio of ηN channel, as well as the harmonic oscillator strength of the quark model are treated as parameters and determined by the fits. The quark model symmetry breaking could introduce contributions from the resonance $S_{11}(1650)$ and $D_{13}(1600)$, which have been suppressed in the $SU(6)\otimes O(3)$ symmetry limit due to the Moorhouse selection rule [18]. Although an explicit consideration of such a breaking has not

been done here, a possible influence of these resonances could have been contained in those fitted quantities as a background contribution. In this sense, the 15% uncertainty for the $\eta N S_{11}(1535)$ coupling can be regarded as a reasonable estimation. Another feature of this approach is that the Lorentz boost factor in the equal velocity frame (EVF) succeeds in the description of the $S_{11}(1535)$ form factor. Therefore, an *ad hoc* form factor is avoided.

We have shown that the extracted parameters are compatible with their values coming from previous independent works. The cross section data for both photo- and electroproduction are well reproduced. Explicitly, it shows that the electroproduction process indeed provides us with rich information. It sheds light on the $\eta N S_{11}(1535)$ coupling, which had not been well-determined in the real photon reaction. Although the scalar coupling of the longitudinal photon is found to be larger than that reported in Ref. [35], we succeed in removing the model-dependent uncertainties arising at the electromagnetic interaction vertex ($\gamma_{(v)} p \rightarrow S_{11}$) from the transition amplitude $\gamma_{(v)} p \rightarrow S_{11} \rightarrow \eta p$ for the $S_{11}(1535)$. The derived simple relation (Eq. 37) thus provides a constraint on the $\eta N S_{11}$ coupling with an uncertainty of about 15%. This could be the first explicitly constrained estimation of the $S_{11}(1535)$ properties in theory. Such a result might lead us to the conclusion that the main component in the $S_{11}(1535)$ wave function is rather like a non-exotic three-quark state than a $K\Lambda$ ($K\Sigma$) bound state [44]. Possible configurations from the latter should be small at the $S_{11}(1535)$ energy, if exists.

It should be noted that this calculation was done before the publication of a new set of data from the CLAS Collaboration [45]. The S_{11} helicity amplitude $A_{\frac{1}{2}}$ for $0.25 \leq Q^2 \leq 1.5$ (GeV/c)² has been significantly improved by that experiment. Their results, which are highly model-selective, shows in good agreement with our calculations.

ACKNOWLEDGMENTS

We are grateful to the GRAAL collaboration, especially J.-P. Bocquet, D. Rebreyend, and F. Renard for having provided us with their data prior to publication. We wish to thank

J.-P. Didelez, M. Guidal and E. Hourany for useful discussions concerning the GRAAL experiments and S. Dytman, B. Ritchie and P. Stoler for helpful exchanges on the measurements performed at JLab. This work is supported by the “Bourses de Recherche CNRS-K.C. WONG” and IPN-Orsay.

REFERENCES

- [1] B. Krusche *et al.*, Phys. Rev. Lett. **74**, 3736 (1995).
- [2] A. Bock *et al.*, Phys. Rev. Lett. **81**, 534 (1998).
- [3] A. Ajaka *et al.*, Phys. Rev. Lett. **81**, 1797 (1998).
- [4] F. Renard *et al.*, (The GRAAL Collaboration), hep-ex/0011098.
- [5] G. Knöchlein, D. Drechsel, and L. Tiator, Z. Phys. A **352**, 327 (1995).
- [6] Z.-P. Li, Phys. Rev. C **52**, 4961 (1995).
- [7] M. Benmerrouche, N.C. Mukhopadhyay, and J.F. Zhang, Phys. Rev. Lett. **77**, 4716 (1996).
- [8] Z.-P. Li and B. Saghai, Nucl. Phys. **A644**, 345 (1998).
- [9] N.C. Mukhopadhyay and N. Mathur, Phys. Lett. B **444**, 7 (1998).
- [10] L. Tiator, D. Drechsel, G. Knöchlein, and C. Bennhold, Phys. Rev. C **60**, 035210 (1999).
- [11] R.M. Davidson, N. Mathur, and N.C. Mukhopadhyay, Phys. Rev. C **62**, 058201 (2000).
- [12] Z.-P. Li, H.-X. Ye, and M.-H. Lu, Phys. Rev. C **56**, 1099 (1997).
- [13] M. Warns, H. Schroder, W. Pfeil, and H. Rollnik, Z. Phys. C **45**, 613 (1990).
- [14] G.A. Warren and C.E. Carlson, Phys. Rev. D **42**, 3020 (1990); C.E. Carlson and C.D. Carone, Phys. Rev. D **58**, 053005 (1998).
- [15] C.S. Armstrong *et al.*, Phys. Rev. D **60**, 052004 (1999).
- [16] N. Isgur and G. Karl, Phys. Rev. D **18**, 4187 (1978); *ibid* D **19**, 2653 (1979); R. Koniuk and N. Isgur, *ibid* D **21**, 1868 (1980).
- [17] A. Manohar and H. Georgi, Nucl. Phys. **B234**, 189 (1984).
- [18] R.G. Moorhouse, Phys. Rev. Lett. **16**, 772 (1966).

- [19] R. McClary and N. Byers, Phys. Rev. D **28**, 1692 (1983).
- [20] F.E. Close and Z.-P. Li, Phys. Lett. **B 289**, 143 (1992).
- [21] Z.P. Li and F.E. Close, Phys. Rev. D **42**, 2207 (1990); F.E. Close and Z.P. Li, *ibid* D **42**, 2194 (1990).
- [22] M. Goldberger and S.B. Treiman, Phys. Rev. **110**, 1478 (1958).
- [23] B. Saghai and Z.-P. Li, Eur. Phys. J. **A 11**, 217 (2001).
- [24] H. Garcilazo and E. Moya de Guerra, Nucl. Phys. **A562**, 521(1993).
- [25] S. Nozawa and T.-S.H. Lee, Nucl. Phys. **A513**, 511 (1990); *ibid* **A513**, 543 (1990).
- [26] C.G. Fasano, F. Tabakin, and B. Saghai, Phys. Rev. C **46**, 2430 (1992).
- [27] F. Fostor and G. Hughes, Z. Phys. C **14**, 123 (1982).
- [28] F. Ravndal, Phys. Rev. D **4**, 1466 (1971).
- [29] U. Beck *et al.*, Phys. Lett. B **51**, 103 (1974).
- [30] L. Tiator, C. Bennhold, and S.S. Kamalov, Nucl. Phys. **A580**, 455 (1994); C. Bennhold, L. Tiator, and S.S. Kamalov, *ibid* **A585**, 313c (1995).
- [31] S.-L. Zhu, Phys. Rev. C **61**, 065205(2000).
- [32] D.M. Manley and E.M. Saleski, Phys. Rev. D **45**, 4002 (1992).
- [33] A.M. Green and S. Wycech, Phys. Rev. C **55**, R2167 (1997).
- [34] Particle Data Group, C. Caso *et al.*, Euro. Phys. J. C **3**, 1 (1998).
- [35] H. Breuker, *et al.*, Phys. Lett. **74B**, 409 (1978).
- [36] F.W. Brasse *et al.*, Z. Phys. C **22**, 33 (1984).
- [37] P. Stoler, Phys. Rep. **226**, 103 (1993).

- [38] F.W. Brasse *et al.*, Nucl. Phys. **B139**, 37 (1978).
- [39] C.E. Carlson and J.L. Poor, Phys. Rev. D **38**, 2758 (1988).
- [40] J.-C. Adler *et al.*, Nucl. Phys. **B91**, 386 (1975).
- [41] F.W. Brasse *et al.*, Nucl. Phys. **B110**, 413 (1976).
- [42] N. Isgur and C.H.L. Smith, Phys. Rev. Lett. **52**, 1080 (1984).
- [43] A.V. Radyushkin, Nucl. Phys. **A527**, 153c (1991).
- [44] Z.-P. Li and R. Workman, Phys. Rev. C **53**, R549 (1996).
- [45] R. Thompson *et al.*, (The CLAS Collaboration), Phys. Rev. Lett., **86**, 1702 (2001).

TABLES

TABLE I. Extracted values for parameters of this model. Detailed discussions are given in the text.

α_η	α (MeV)	$\Gamma_{S_{11}}$ (MeV)	$b_\eta(S_{11})$	$C_{S_{11}}$	$C_{D_{13}}$	$C_{S_{11}}^L$	χ^2
0.10 ± 0.01	384.5 ± 0.2	143.3 ± 0.2	0.55 ± 0.01	1.20 ± 0.30	-0.92 ± 0.03	0.65 ± 0.01	2.36

TABLE II. Extracted total width $\Gamma_{S_{11}}$ and partial decay width $\Gamma_\eta^a \equiv b_\eta \Gamma_{S_{11}}$ and $\Gamma_\eta^b \equiv \alpha_{S_{11}} \chi$ for the $S_{11}(1535)$. Corresponding estimations by the Particle Data Group [34] are also listed.

	$\Gamma_{S_{11}}$ (MeV)	Γ_η^a (MeV)	Γ_η^b (MeV)
This work	143.3 ± 0.2	78.8	89.4
PDG	150	75.0	-

FIGURES

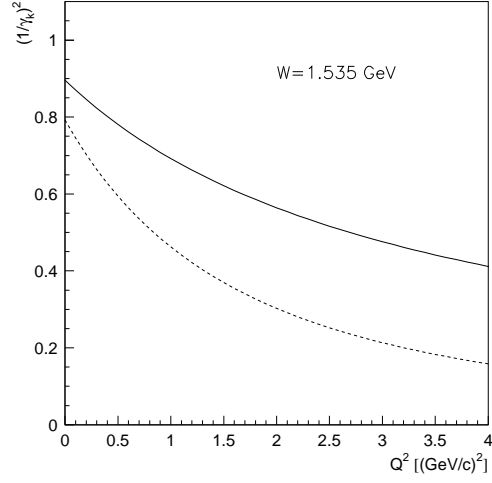


FIG. 1. The Q^2 -dependence of the Lorentz boost factor in the EVF (solid) and meson-nucleon c.m. frame (dashed), respectively.

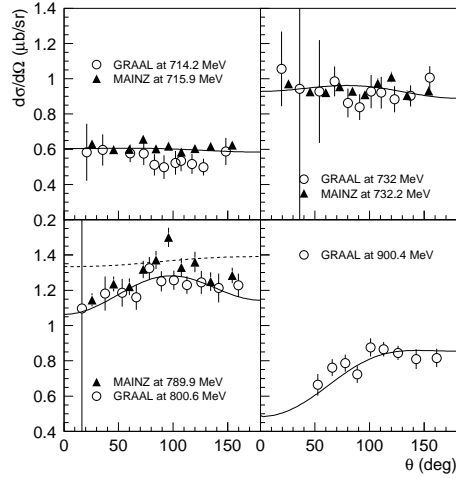


FIG. 2. Differential cross sections in the real photon limit. Solid curves denote the fitting results, while the dashed curve denotes the result in the absence of the $D_{13}(1520)$. Data are from Mainz [1] (triangles) and GRAAL [4] (circles).

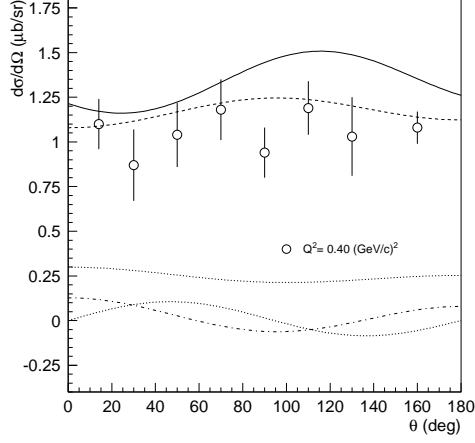


FIG. 3. Differential cross section at $Q^2 = 0.4 \text{ (GeV/c)}^2$ with $\phi_\eta^* = 0^\circ$. The solid curve comes from the global fits. Different components of the cross section are also presented: the dashed curve for $d\sigma_T/d\Omega^*$; the dotted for $d\sigma_L/d\Omega^*$; the dot-dashed for $d\sigma_{TT}/d\Omega^*$; and the heavy-dotted for $d\sigma_{TL}/d\Omega^*$. Data are from Ref. [29].

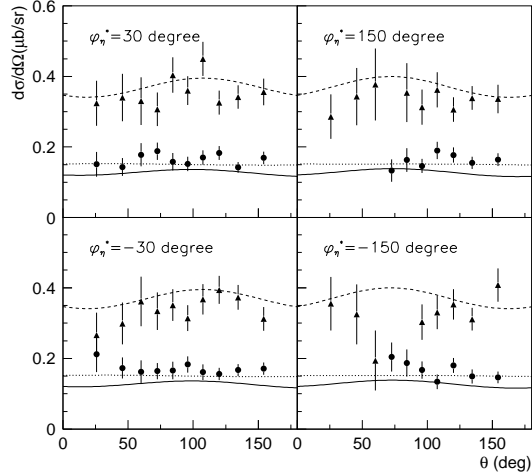


FIG. 4. Fitting results for the differential cross sections at $Q^2 = 2.4$ (dashed) and 3.6 (GeV/c)^2 (solid) for different ϕ_η^* . The dotted curves are calculations without $D_{13}(1520)$ contributions at $Q^2 = 3.6 \text{ (GeV/c)}^2$. Data are from Ref. [15]. The triangles are data at $Q^2 = 3.6 \text{ (GeV/c)}^2$, while the full dots are data at $Q^2 = 2.4 \text{ (GeV/c)}^2$.

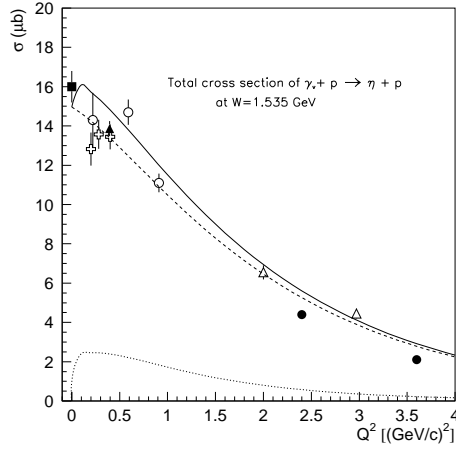


FIG. 5. The Q^2 -dependence of the total cross sections (solid curve). The total transverse and longitudinal cross sections are also shown by the dashed and dotted curves, respectively. Data come from Refs. [1,29,38,15,40,36].

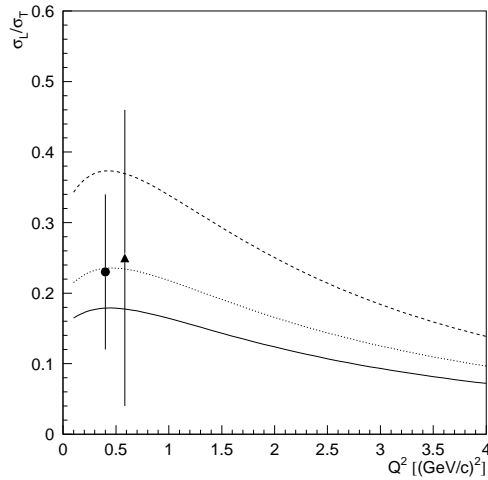


FIG. 6. The Q^2 -dependence of the ratio of σ_L/σ_T . The solid and dotted curves correspond to $C_{S11}^L = 0.65$ and 0.70 , respectively, while the dashed curve is for $C_{S11}^L = 1$. The full circle is from Ref. [35] and the triangle from Ref. [36].

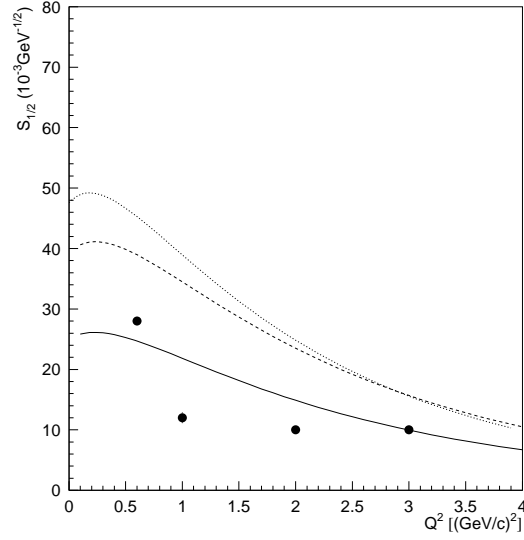


FIG. 7. Longitudinal helicity amplitude $S_{\frac{1}{2}}$ for $S_{11}(1535)$. The solid curve and dashed curves are calculated with $C_{S_{11}}^L = 0.65$ and $C_{S_{11}}^L = 1$, respectively, by Eq. 31, while the dotted curve is given by Eq. 34.

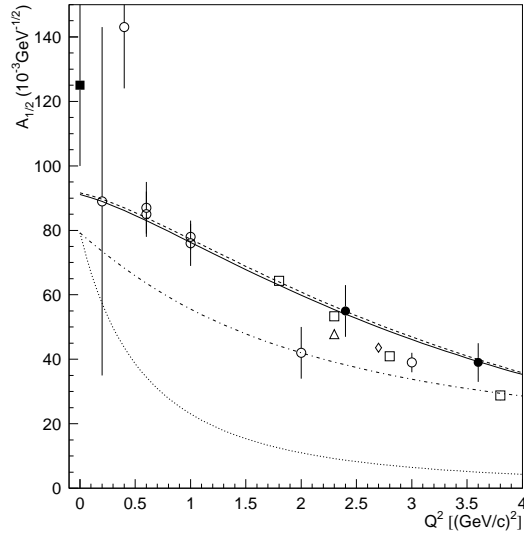


FIG. 8. Transverse helicity amplitude $A_{\frac{1}{2}}$ for the $S_{11}(1535)$. The solid and dashed curves are calculated by Eqs. 40 and 39, respectively. The dot-dashed curve is calculated based on the Lorentz boost factor in the meson-nucleon c.m. frame, and the dotted curve based on a dipole form factor. The full circles are from Ref. [15] and other data points from Refs. [1,37,41].

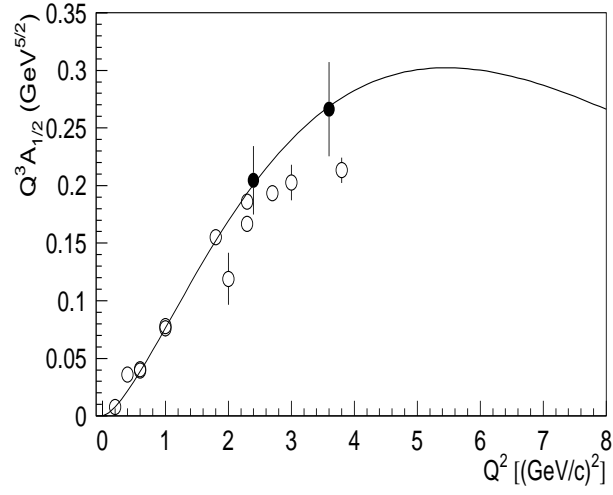


FIG. 9. The quantity $Q^3 A_{\frac{1}{2}}(Q^2)$ calculated in this model. The full circles are from Ref. [15] and the empty ones from Refs. [1,37,41].